1

Negative Electrodes

1.1. Preamble

There are three main groups of negative electrode materials for lithium-ion (Li-ion) batteries, presented in Figure 1.1, defined according to the electrochemical reaction mechanisms [GOR 14].

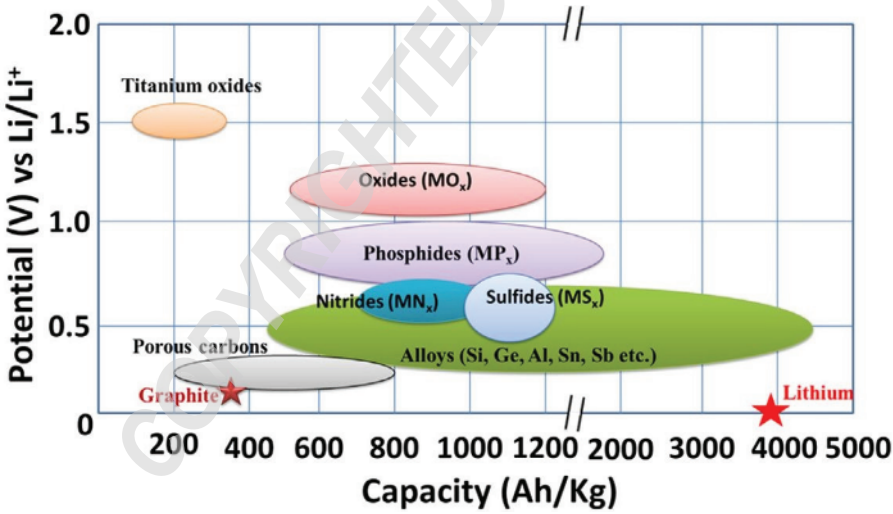

Figure 1.1. *Negative electrode materials put forward as alternatives to carbon graphite, a comparison of their respective capacities and potential. From [ZHE 95]*

The materials known as insertion materials are Li-ion batteries' "historic" electrode materials. Carbon and titanates are the best known and most widely used and will be described in section 1.3. These insertion materials display the advantage of undergoing little structural change during the successive exchanges of Li^+ ions when the battery is charged and discharged (graphite has a volume expansion of 11%). On the contrary, the number of Li^+ inserted is limited, which gives rise to relatively weak capacities (Figure 1.1).

Studies on how to increase batteries' energy (and therefore, capacity) and their power have aimed for some years to increase the number of Li reversibly inserted into the electrode material (or active material, AM). To this end, new AMs have been synthesized. Electrode formulations (which consist of a mixture of AM with a polymer binder and a carbon conducting additive, all in the form of a film) have also been much studied since they are vital to obtaining better electronic and ionic conduction properties in the electrode. Among these new electrode materials, the alloy and conversion-type materials display very high specific theoretical capacities (up to 3,578 mAh/g) compared to insertion materials, correlated with a reaction with a larger amount of lithium. The electrochemical mechanisms are, therefore, of a biphasic type since the starting phase is transformed into another (lithiated) phase with a different crystalline structure (Figure 1.2). These materials' weak point lies in the electrode's volume expansion, correlated with the phase transformation taking part during the AM's reaction with the lithium, leading to volume changes of 200–300%.

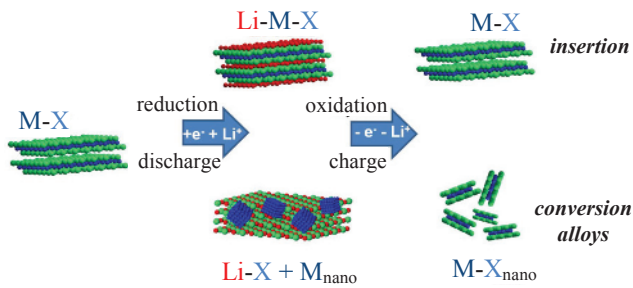

Figure 1.2. *Electrochemical mechanisms of different negative electrode materials, of insertion-type (above), or alloys and conversion-type (below). For a color version of the figure, see www.iste.co.uk/dedryvere/electrodes.zip*

Section 1.2 introduces the insertion materials, (1) briefly discussing carbon graphite's electrochemical properties (since these are widely discussed in the literature), carbon graphite is the standard material at the negative electrode of commercialized Li-ion batteries, and then (2) the most studied titanium oxides.

Section 1.3 displays in more detail the alternatives to carbonaceous materials, which are the alloys, and continues to the conversion materials.

1.2. Classic materials: insertion mechanism

1.2.1. *Graphitic carbon*

1.2.1.1. *Lithium intercalation mechanisms*

Graphite (C_{gr}) is one of the allotropic forms of carbon which is characterized by a tridimensionally ordered structure made up of graphene planes organized at regular intervals along the c axis. The very different nature of the C-C bonds in the plane and between planes, covalent for the former and Van der Waals-type for the latter, leads to a very good intercalation material, especially for lithium. The chemical intercalation of lithium into graphite was discovered in the 1950s [HER 55]. This intercalation leads to the formation of phases known as nth stage, the stage's value n represents the number of layers of carbon separating two successive intercalate layers.

It was during the 1980s that the reversible electrochemical intercalation of lithium into graphite was demonstrated for the first time, by using a polymer electrolyte. The first patent was placed in the USA by Bell Labs, on a reversible system C_{gr}//Li in an organic liquid electrolyte [BAS 83]. These results enabled the rapid conversion of a rechargeable lithium battery, unstable due to the formation of dendrites between the two electrodes, into a stable rechargeable Li-ion battery, known as a "rocking-chair" with the exchange of lithium between the two insertion electrodes, the negative and the positive [YAZ 83, TOU 77]. The formation of these stages (or graphite intercalation compound (GIC) for an intercalation compound of graphite) is electrochemically characterized by the presence of different plateaux of potential on the galvanostatic curve C_{gr}//Li (Figure 1.3(b)). Lithium, through a transfer of charge, is inserted into graphite to form the phases Li_xC_6 ($x \leq 1$). This electrode has a potential between 100 and 200 mV versus Li. The GICs

possess a very high electronic conductivity, which enables an excellent transfer of charge during the electrochemical intercalation of Li, as well as an easy structural expansion in the *c* direction (weak Van der Waals bonds) facilitating the diffusion of Li in the sheets, even at high rate. Research into this system intensified at the beginning of the 1990s, particularly in Japan, later leading Sony [NAG 91] and other businesses to introduce Li-ion batteries to the portable electronics market.

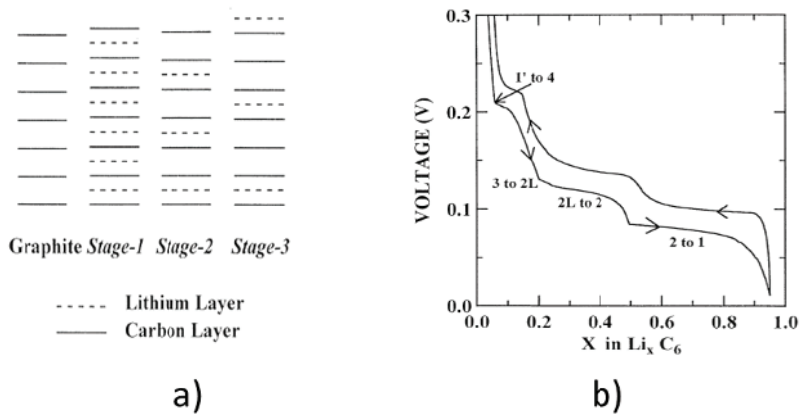

Figure 1.3. *a) Diagram of stages of graphite intercalated by lithium, b) galvanostatic curve for a battery C_{gr}//Li making the correspondence between plateaux of potential and stages formed. (Adapted from [ZHE 95] with permission. Copyright 1995 American Physical Society)*

1.2.1.2. *Electrode/electrolyte interface and additives*

Like all AMs whose potential is less than the electrolyte's reduction potential, graphite can only perform as a negative electrode material due to the formation of a passivation layer (solid electrolyte interphase (SEI)) that is stable over time and over the cycle's course. However, in the particular case of carbonaceous materials, whose operating principle rests on the reversible insertion of Li^+ ions between the graphene sheets, this SEI plays another fundamental role. In fact, when the Li^+ ions are intercalated, these should first shed their solvation sphere before being inserted into the sheets. However, sometimes it happens that they are inserted with their solvation sphere, which the layered structure of carbonaceous material cannot tolerate (Figure 1.4). The graphene sheets are then irreversibly separated, destructuring the material, which is termed the exfoliation phenomenon,

leading to a rapid drop in electrochemical performance. A careful choice of a mixture of electrolyte solvents enables the formation of an SEI impermeable to solvent molecules in order to avoid this co-intercalation (Figure 1.4). In particular, ethylene carbonate (EC) has been shown to be indispensable to forming a protective layer on graphite, whereas propylene carbonate (PC) has an adverse effect. SEI formation mechanisms through the reduction of electrolyte solvents have been widely discussed in the literature. They lead in particular to the deposition of solid carbonates (Li_2CO_3, $ROCO_2Li$, etc.) in an especially complex mixture of formed products [XU 04].

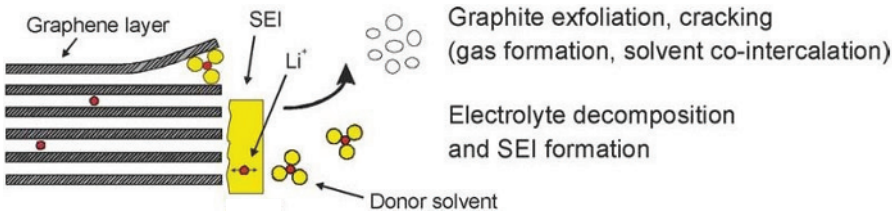

Figure 1.4. *Graphite exfoliation process resulting from the co-intercalation of the solvent between the graphene sheets (above). Protective role of the passivation layer (SEI) which blocks the exfoliation (below). (Adapted from [VET 05] with permission. Copyright 2005 Elsevier)*

The formation of an SEI with good electric (electronically isolating and ion-conducting) and mechanical properties (flexible and able to accompany volume changes in the electrode) and a good stability upon cycling is so important for the performance and life of Li-ion batteries that additives are added to the electrolyte expressly to this end [XU 14a]. When the battery is charging, an additive whose reduction potential is greater than that of the solvent will reduce preferentially at the negative electrode's surface. If the film is polymeric, it will give the SEI better mechanical properties than an SEI formed by the simple reduction of the solvents. This is why the vinyl function –CH = CH-, which is easily polymerizable, is often found in these additives.

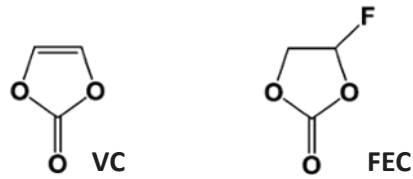

Figure 1.5. *Vinylene carbonate (VC) and fluoroethylene carbonate (FEC): two electrolyte additives for SEI formation currently used in Li-ion batteries*

Among these, vinylene carbonate (VC) is without doubt the most used currently and is present in most systems on the market today (Figure 1.5) [SIM 97]. Fluoroethylene carbonate (FEC), another additive which is becoming increasingly important today, does not contain the vinyl function. However, during its reduction at the electrode's surface, it is transformed into VC, producing lithium fluoride LiF, to follow the same polymerization process [ETA 11]. Other types of additives have also been widely studied, such as those containing sulfur, boron or even the isocyanates [ETA 11]. The combination of several additives is also of interest for improving batteries' performances, for example, the combination of VC and FEC. However, the action mechanisms for these additives are not always very clear, particularly when they combine.

In conclusion, today the formation of the SEI on carbonaceous materials can easily be controlled due to an optimized formulation of the electrolyte and the use of additives. For this reason, graphite still forms the majority of the more than 10 billion Li-ion batteries produced each year. However, these batteries' capacity (which depends directly on the properties of the electrode materials) remains limited, mainly as a result of the capacities, limited to 372 mAh/g and 820 mAh/cm^3, of the Cgr negative electrode. It is essential to turn to new negative electrode materials to increase gravimetric and volumetric capacities. Moreover, carbonaceous materials pose a safety problem since their potential is very close to that of the Li^+/Li couple, leading to a risk of metallic lithium deposits building up at the electrode's surface rather than an insertion of Li^+ ions between the graphite sheets (in particular, during rapid charging). This problem is a handicap for future applications, in particular for those in which safety considerations are paramount (in particular, electric vehicles). This is why over the last 15 years, research has turned to new materials. However, electrode/electrolyte interfaces made up of these new materials are still poorly mastered today.

1.2.2. *Titanium oxides*

Titanium oxides, another type of insertion material, have been much studied for use in batteries, by replacing Cgr. Like graphite, they present very interesting lithium insertion properties with a good reversibility, good kinetics and a good thermal stability (especially for $Li_4Ti_5O_{12}$ (LTO)). Moreover, they are benign for the environment and adapted to low-cost mass production.

Lithium insertion into titanium oxides plays on the redox couple Ti^{4+}/Ti^{3+} at a potential of between 1.3 and 1.9 V versus Li/Li^+, depending on the polymorph. This potential window means that (1) safety risks linked to metallic lithium deposits can be avoided (intervening at 0 V) and (2) the copper collector can be replaced by less costly aluminum.

1.2.2.1. *$Li_4Ti_5O_{12}$*

Compared to carbon (and even more so compared to alloys and conversion materials), spinel-type $Li_4Ti_5O_{12}$ (LTO), described in Figure 1.6 ($Li_{4/3}Ti_{5/3}O_4$ or even $(Li)_{Td}(Li_{1/3}Ti_{5/3})_{Oh}O_4$, Td and Oh, respectively, for tetrahedral and octahedral sites), is considered to be a material free from constraints, since practically there is no volume change during charge/discharge cycles, during the reversible transformation of LTO into $Li_7Ti_5O_{12}$ (rocksalt structure), which enables a good stability during the cycle to be guaranteed, even at high rate. It is an easy and relatively cheap synthesis and its constant potential of the order of 1.5 V, which makes it safe, makes this material the titanium oxide most used for industrial research [ALT 15, SCI 09] and for varied applications, especially portable ones, despite its weak gravimetric capacity (175 mAh/g) compared to that of graphite.

However, the main problem with this material is that it generates gas during cycling, combined with a loss of capacity, particularly at high temperature, which is an obstacle to its commercial use [BEL 12, WU 12]. The gas emitted is partly made up of hydrogen and CO_2, involving a decomposition of the carbonated solvents and the participation of traces of water present in the electrolyte [BER 14]. The reason for this reactivity of $Li_4Ti_5O_{12}$ is due to its surface state, especially to the presence of holes in the (111) oriented surfaces' electronic structure, responsible for the oxidation of solvent molecules that leads to the emission of CO_2 [KIT 14]. Recent studies show that the problem of reactivity with the electrolyte can in part be

resolved by modifying the LTO particles through the application of an inorganic coating, for example, AlF_3, which improves its performance during cycling (see Figure 1.7) [LI 14b].

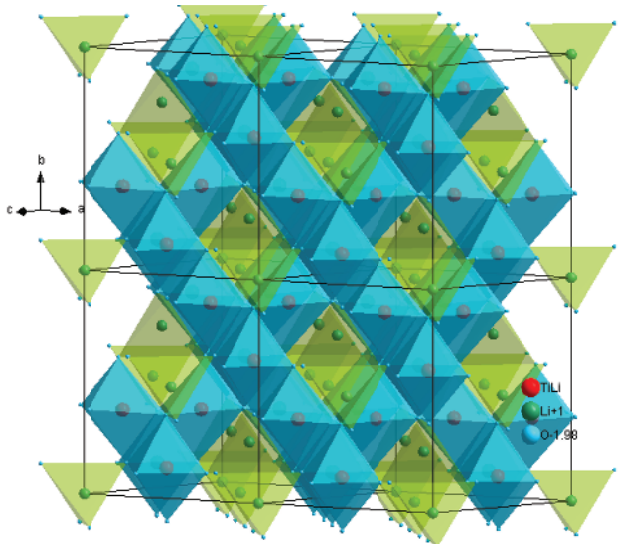

Figure 1.6. *Diagram of the structure $Li_4Ti_5O_{12}$ ($[Li]_{8a}[Li_{1/3}Ti_{5/3}]_{16d}O_4$, described in the space group Fd-3m), the tetrahedra LiO_4 are in light gray and the octahedra are in dark gray (Li/Ti)O6. For a color version of the figure, see www.iste.co.uk/dedryvere/electrodes.zip*

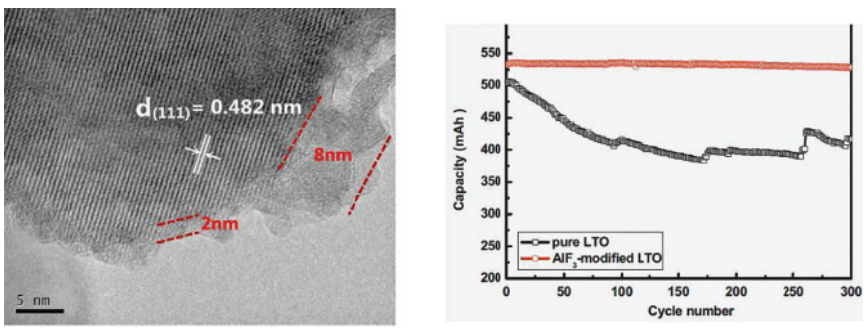

Figure 1.7. *Image of a $Li_4Ti_5O_{12}$ particle with AlF_3 coating, obtained from transmission electron microscopy (TEM). Performance during cycling of $LiMn_2O_4$//$Li_4Ti_5O_{12}$ batteries with and without coating. (Adapted from [ZHE 09] with permission. Copyright 2014 Elsevier)*

1.2.2.2. TiO_2

There are numerous types of titanium dioxides listed and in the vast majority titanium is found in octahedral coordination of oxygen. TiO_2's different structures vary depending on the way the TiO_6 octahedra are combined by edges and/or corners (Figure 1.8).

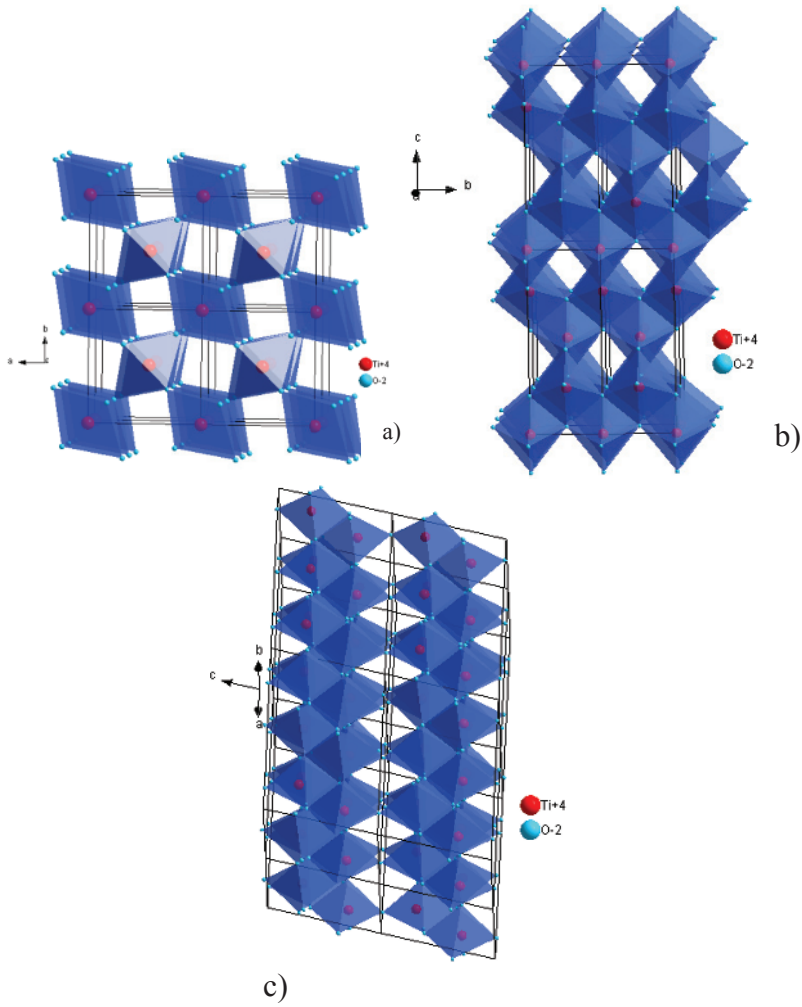

Figure 1.8. *Diagram of TiO_2 structures a) rutile described in space group $P4_2/mnm$, b) anatase described in space group I 4/amd and c) bronze (B) described in space group C^2/m. For a color version of the figure, see www.iste.co.uk/dedryvere/electrodes.zip*

1.2.2.3. *Different crystallographic arrangements*

In the TiO_2 rutile structure, each TiO_6 octahedron shares two opposing edges with the adjacent octahedra to form chains along the ***c*** axis (Figure 1.8(a)) linked to each other by corners. The oxygen planes and the titanium-vacancy planes are separated by a small distance of 1.148 Å, which is responsible for the highest density (d = 4.2g/cm^3) of all TiO_2 polymorphs. The vacancies in the titanium network cause tunnels with a squared section along the (001) direction. In the case of anatase, the TiO_6 octahedra are linked by the edges to form chains along the ***a*** axis (Figure 1.8(b)). The chains are linked by sharing the octahedra's corners (along the ***b*** axis) which themselves combine along the ***c*** axis by sharing the edges to form a three-dimensional (3D) network. Oxygen atom planes and titanium/vacancies planes are separated by a distance of 1.17 Å, significantly higher than that observed in rutile, which is responsible for a lower density (d = 3.92 g/cm^3). The vacancies in the cationic planes cause tunnels to appear following the directions (100) and (010). TiO_2 (B) is organized by a face centered cubic stacking of type NaCl (space group C2/m) (Figure 1.8(c)). Its structure is more open and less dense (d = 3.64 g/cm^3) than that of anatase and rutile. Tunnels following the two directions *b* and *c* facilitate the diffusion of lithium.

1.2.2.4. *Performances and mechanisms*

The theoretical capacity of TiO_2 is nearly double that of LTO with 336 mAh/g corresponding to the insertion of one mole of Li per mole of TiO_2, and the complete reduction of Ti^{4+} into Ti^{3+}, which makes it an interesting alternative to LTO. Nevertheless, its experimental capacities are limited by several phenomena described below, and this is especially true for rutile. Anatase and TiO_2(B) are considered to have the most potential for anodes in this family because of their rapid insertion-extraction kinetics and higher capacity.

The anatase phase, for a long time considered as the most electrochemically active polymorph, [ZAC 88, ZHE 09] has a discharge potential around 1.8 V versus Li and displays a complex insertion mechanism in three stages [WAG 07]: an initial Li insertion process according to a solid solution mechanism, then a biphasic transformation process from the initial phase to a phase crystallizing in an orthorhombic space group which corresponds to a distortion in the Ti's octahedral coordination sphere and finally a solid solution-type insertion reaction. This

reversible mechanism is accompanied by a limited volume expansion of the network of 4% [BEH 12]. The experimental electrochemical insertion of 0.6 Li (200 mAh/g) into TiO_2 anatase, at an average potential of 1.78 V, is far from the 1 Li theoretically expected, and this is due to the limited electronic conductivity (10^{-12}-10^{-7}S/cm), as well as the weak diffusion coefficient of Li^+ (10^{-15}–10^{-9} cm^2/s).

TiO_2(B), which has been the focus of much recent research, has the same theoretical capacity as anatase but has a weaker average potential of 1.5 V, which allows a higher energy density to be expected for the full battery. There is still some debate in the literature on the most stable insertion sites for Li, and on the exact mechanism [MOR 12]. Classically, a $Li_{0.9}TiO_2$ composition is reported during the first discharge corresponding to 305 mAh/g and 0.7 Li is then exchanged reversibly. Recent studies have shown that this material shows excellent cyclability in Li-ion systems versus a $LiMn_2O_4$ cathode (a 120 mAh/g capacity is reached over 1,000 cycles at a current density of 150 mA/g for a potential of 2.5 V) [ARA 13].

1.2.2.5. *Optimizations*

For these three TiO_2 polymorphs, it has been shown that capacity depends strongly on morphological properties. The methods explored for improving the performances of TiO_2 phases aim to (1) increase the ionic conductivity, which is limited through a weak diffusion coefficient in a solid state, (2) increase the electronic conductivity, which results from a lack of electrons in the conduction band ($3d^0$) combined with a wide gap (3 *eV*) and (3) decrease the high irreversible capacity during the first cycle in line with the electrolyte's instability. The nanostructuration enables the diffusion paths to be reduced and diffusion in the solid state and, consequently, the insertion of Li in TiO_2 to be improved. In the case of TiO_2 rutile, such an approach has enabled the specific capacity to be increased (e.g. 190 mAh/g for a very slow rate of 0.067 mA/g) nevertheless, the cyclability remains limited [KUB 09]. For anatase, as illustrated in Figure 1.9, nanostructuring TiO_2 samples heavily impact the shape of the galvanostatic curves as well as the number of Li inserted, which can then become closer to the 1 Li theoretically expected. In this case, the particles' reduction in size extends the length of the 1.5 V potential plateau, while the increase in the surface area and porosity of the sample increases up to 0.5 Li the number of lithium inserted in the lower potential region (interfacial storing) due to a raised contact zone between the AM and the electrolyte. Nevertheless, the Li inserted at low potential is often

partly due to electrolyte degradation, a process which is favored by the large surface area of the sample, and thus this is only partially reversible.

Several studies carried out on nanometric samples of anatase and TiO_2(B) showing the same surface area highlight the kinetic advantages of TiO_2(B) attributable to its structural properties (the opening of channels) and its pseudo-capacitive properties (that is to say, the lithiation reaction of TiO_2(B) generates a current proportional to the scan potential rate, characteristic of a phenomenon not limited by the diffusion of Li) [WIL 09]. These improved performances at high rates are favored by high surface areas and favorable surface energies. These properties enable a more rapid cycling and so a capacity of 80 mAh/g has been maintained at a 10 C rate (3,350 mAg^{-1}) over 5,000 cycles [HAS 11].

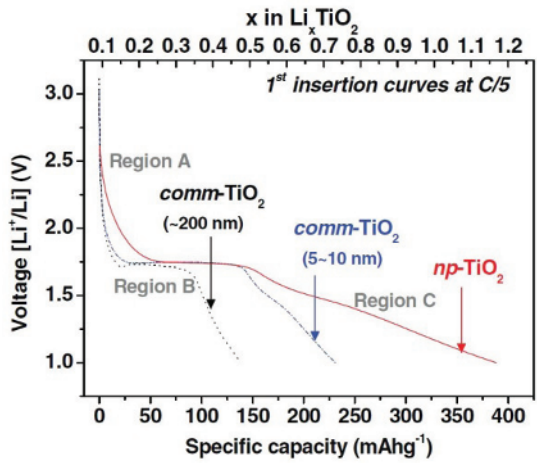

Figure 1.9. *First galvanostatic discharges of anatase samples: two commercial samples showing two particle sizes (200 and 5–10 nm) and a nanoporous sample. (Reprinted from [SHI 11] with permission. Copyright 2011 WILEY-VCH Verlag GmbH & Co)*

With the same aim, synthesizing mesoporous TiO_2 has been suggested to improve performances, but this also results in the interfacial insertion of Li being increased, more or less reversibly. These complex and costly methods of synthesis are difficult to organize on a large scale and the volumetric energy density of such electrodes remains low due to the low density of TiO_2.

The use of dopants or the formation of composites with carbon or other conductive components can be effective for increasing the weak intrinsic conductivity of TiO_2 (10^{-12} to 10^{-7} S/cm). This approach has largely been proven in the domain of photocatalysis for adjusting the absorption window, by doping with aliovalent cations leading to the creation of holes or electrons depending on whether the cation is acceptor or donor. By manipulating the chemistry of defects in TiO_2, it is thus possible to adjust electronic properties and enhance electrochemical performances, especially at high rates [GRO 15, FEH 13].

1.3. Toward other materials and other mechanisms

The alloys that are formed electrochemically by a reaction between lithium and a metal (or semi-metal) such as Sn, Si, Sb or Al theoretically enable capacities more than 10 times greater than that of C_{gr} to be expected, 783 mAh/g for SnO_2 and 3,578 mAh/g, for example, for silicon (Figure 1.10).

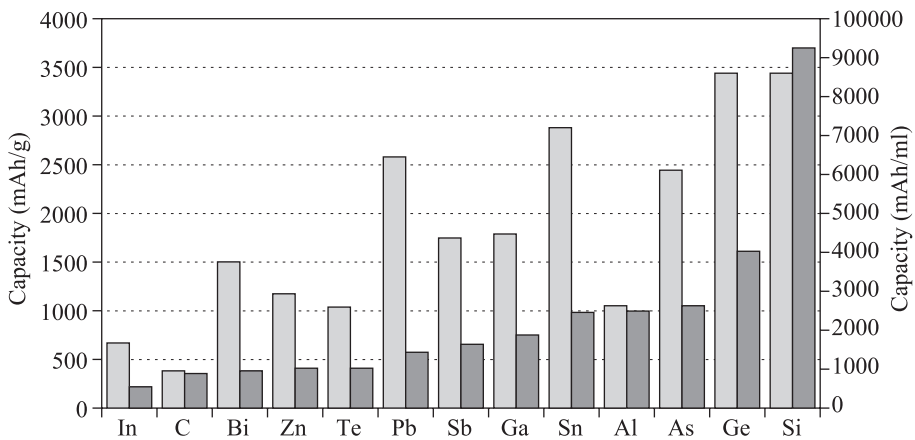

Figure 1.10. *Gravimetric and volumetric capacities of different LiX alloys, X being an element from columns 12 to 15 of the periodic table. (Reprinted from [LAR 07] with permission. Copyright 2007 the Royal Society of Chemistry)*

These materials' main limitation is their great volume change during insertion/de-insertion reactions (for example, the transformation from Sn to $Li_{4.4}Sn$ is combined with a more than four-fold increase in the initial lattice volume) which is responsible for a loss of contact between the grains and the

current collector, a significant, irreversible loss of capacity in the first cycle and a limited lifespan. A great deal of research has been carried out to try to limit these effects by reducing the size of the particles from micron scale to nanoscale and by making composite compounds (mixtures of electrochemically active and inactive materials), in order to buffer the volume changes. Nanostructuring the electrodes is also an efficient means of improving this type of electrode's capacity, lifespan and kinetics.

In 2005, these optimizations enabled SONY to market batteries containing Sn–Co nanoparticles in a carbon matrix as a negative electrode [TOD 07]. In this case, the carbon matrix buffers the volume expansion during the formation of the Li_xSn alloys. This battery permits a 30% increase in capacity (from 710 to 910 mAh for a 14430-type cell) and a 20% increase in volumetric energy density) even at high rates, compared to the classic $C_{gr}/LiCoO_2$ battery.

1.3.1. *Silicon*

Silicon, the second most common element on the Earth, is inexpensive and benign for the environment. Due to the existence of numerous Li_xSi phases, demonstrated electrochemically by Huggins *et al*. [BOU 81] in 1981, silicon has been the most promising alternative to carbon. Indeed, these highly lithiated phases enable very high gravimetric capacities to be reached (3,578 mAh/g for $Li_{15}Si_4$). Moreover, silicon's discharge potential of 0.4 V versus lithium is close to that of graphite which guarantees a high voltage in a Li-ion battery. Silicon, therefore, seems a promising means of equipping the batteries of tomorrow as shown by the development of start-ups such as *Envia Systems* (which achieved record capacities of 400 Wh/kg with a composite anode based on silicon) [ENV 13]. Numerous research groups' enthusiasm with silicon is, therefore, understandable.

Nevertheless, Si's cycling performances are limited, essentially due to the high volume expansion between silicon and the lithiated phases (~300%) and the resulting instability in the passivation layer (SEI).

1.3.1.1. *Lithiation/delithiation mechanisms*

It has become possible to understand Si's lithiation/delithiation mechanisms due to the use of *ex situ* and *in situ* methods. X-ray diffraction (XRD) *in situ*, nuclear nagnetic resonance (NMR), microscopy techniques *in*

situ such as scanning electron microscopy (SEM) and transmission electron microscopy (TEM) play an important role in understanding the evolution of Si electrodes during cycling and degradation processes. The identification of the SEI's formation and evolution during cycling is also vital for performances.

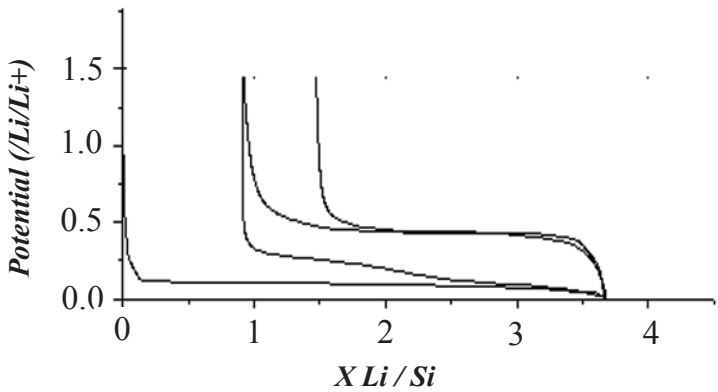

Figure 1.11. *Galvanostatic curve of a composite Si electrode [Si/Cb/CMC] [70/18/12] cycled in the electrolyte $LiPF_6$ in EC:PC:3DMC (+1% FEC)*

These studies have shown that in the potential plateau close to 0.1 V (Figure 1.11) crystalline silicon is amorphized and none of the phases of the binary diagram Li-Si is formed in a crystallized state, except in some particular cases in which a metastable crystalline phase $Li_{15}Si_4$ grows at the end of the discharge at low potential (50 mV). The second discharge (lithiation) is carried out at a higher potential, following a curve characteristic of a solid solution-type mechanism, with two pseudo-plateaux at 0.3 and 0.1 V versus Li^+/Li. NMR studies [KEY 11] have shown that it is necessary to break all the silicon clusters so that the $Li_{15}Si_4$ phase can grow. On the other hand, it has also been shown that the mechanisms during the following charge depend strongly on the possible presence of the $Li_{15}Si_4$ phase. A recent study using microscopy has enabled the (de)lithiation mechanisms in silicon-based electrodes to be studied and understood in more depth using multi-scale observations [ROB 13]. On the level of the Si particle, different mechanisms occur during the first lithiation, according to two factors: the size of the particles and the defects within them. The composition of the Li_xSi alloy has been observed to be weaker in lithium for

nanoparticles than for microparticles. The defects, mainly due to grinding, constitute preferential lithiation sites.

To limit the effects of dramatic volume changes between lithiation and delithiation and the SEI's resulting instability, different strategies have been put in place, such as silicon nano-architecturing, a specific electrode formulation and the use of electrolyte additives as described above for carbonaceous materials.

1.3.1.2. *Nanostructured silicon*

Numerous studies have been carried out on the miniaturization of silicon by nanostructuring from zero-dimensional (0D) (nanoparticles), one-dimensional (1D) (nanotubes and nanowires) to two-dimensional (2D) (thin films) in order to improve performances by increasing lifespan on cycling and the charge kinetics due to (1) improved mechanical properties, (2) raised surface areas and (3) better electronic and ionic transport properties of these nanomaterials [SU 14]. Silicon nanoparticles' (0D) electrochemical performances still remain limited, mainly due to the high volume variation during the charge and discharge processes, responsible for pulverization and loss of contact with the current collectors. In addition, the silicon nanoparticles generally have a poor electronic conductivity. To overcome these problems, the silicon nanoparticles are generally combined with other materials such as porous carbon, carbon nanotubes (CNTs) and graphene to improve their electronic conductivity and structural stability. Thus, excellent performances have been achieved in terms of specific capacity and number of cycles. However, it is often expensive to manufacture these nanomaterials (use of catalyzers or expensive surfactants for relatively low yields) [WU 12a], which make them still far from a realistic application.

Thin 2D silicon films (≈ 50 nm thick) prepared by physical or chemical vapor deposition (CVD) (physical vapor deposition (PVD) and vapor CVD) can deliver impressive capacities of more than 2,000 mAh/g over thousands of cycles, due to better control and limitation of the volume expansion. However, the Si's thickness cannot exceed the limit of 300 nm because this would risk creating fissures in the films, which would then seriously limit the energy density.

Despite these many advances on architectured silicon over the last 10 years, which have enabled battery lifespan to be extended, Si' theoretical capacity to be neared (3,578 mAh/g) and the charge time to be improved,

numerous problems still remain surrounding their application in electric vehicles or for energy storage systems. The main limitation is the low density of nanostructured electrodes, responsible for low volumetric capacities. Different strategies have been put in place to relieve this problem by manufacturing thicker electrodes, but in these instances lifespan is severely affected, and accompanied by a significant polarization. A recent approach consisted of preparing porous silicon using electrochemical engraving. These porous electrodes, which allow a significant thickness of silicon to be electrochemically active, have shown promising performances since in this case a high surface capacity (4 mAh/cm^2) is obtained, enabling the criteria required for application in batteries to be met. Nevertheless, the cyclability remains limited [LI 14a].

1.3.1.3. *Electrode formulation*

A simpler method of obtaining electrodes more loaded with silicon, displaying higher energy densities without compromising on cycling performances, has been to work on electrode formulation, using different polymer binders. The greater efficiency of carboxymethyl cellulose (CMC, an inexpensive food additive soluble in water is very attractive from an environmental point of view) as an electrode binder, compared to classic poly(vinylidene fluoride) (PVdF), has been demonstrated [LES 07, MAZ 09a]. By combining the use of this binder with cycling in a limited potential window (at low potential in order to limit degradation of the electrolyte and volume expansion), better performances in terms of capacity, coulombic efficiency and cyclability have been obtained. Yet, PVdF is known to be more elastic than CMC, which could be a major asset for controlling the volume expansion of the materials forming the Li_xX alloys. The improvement brought by CMC should be correlated with its capacity to connect particles of carbon conducting additives and silicon (covered with a fine layer of SiO_2). This grafting of CMC to the surface of Si particles via an esterification reaction involving the CMC's carboxylic acid functions and the silanol groups of the SiO_2 present on the silicon's surface seems to be favored by the acidity (pH around 3) of the electrode ink's preparation solution [MAZ 09b]. The construction of a polymeric network when the elements are mixed in the solvent gives rise to a significant increase in the electrode's lifespan over hundreds of cycles. Nevertheless, optimizing the electrode formulation is still not enough to reach the desired energy densities because the capacity and cyclability drop rapidly when the electrode becomes thicker (and thus, more loaded in Si). It has also been

suggested that grafting CMC to the surface of Si grains contributes to passivating the grains' surface [MAZ 12]. The carbon additive, added to improve the electronic conductivity, can also be of different natures and improvements which have been obtained by mixing carbon black and vapor grown carbon fibers (VGCF) with the CMC as a binder [BEH 12].

1.3.1.4. *Aging mechanisms*

Upon aging during cycling, silicon electrodes undergo significant structural and morphological changes, governed by the electrode pores' distribution dynamic (Figure 1.12) [RAD 14]. Following repeated particles' volume increases/reductions, the first cycles lead to the formation of large (micrometric) pores initially absent from the electrode. During the following cycles, the passivating layer (SEI), rather than forming only at the particles' surface, will progressively come to fill these micrometric pores. The electrode will continue to function so long as the percolation of Li^+ ions is not interrupted. However, when the phenomenon becomes more accentuated, the Li^+ ions no longer reach all the Si particles, the lithiation becomes inhomogeneous and the loss of capacity is rapid.

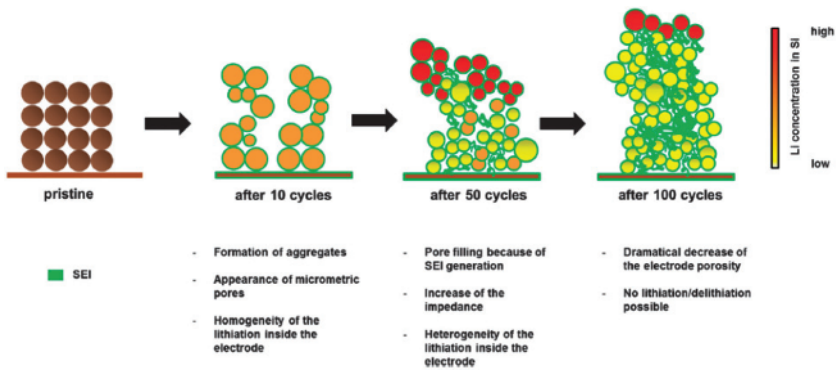

Figure 1.12. *Failure mechanism controlled by the evolution of porosity within the Si electrode. Appearance of large-scale pores (10 cycles). Progressive filling of these pores by products resulting from the electrolyte degradation, making it increasingly difficult for Li^+ ions to percolate. (Reprinted from [PHI 13a] with permission. Copyright 2014. The Owner Societies). For a color version of the figure, see www.iste.co.uk/dedryvere/electrodes.zip*

Particles' surface chemistry also plays a role in aging processes. Beyond the lithiation/delithiation mechanisms within the bulk of the particles leading to the phases described above, the particles' surfaces undergo their own

phase transformations [PHI 12]. The native SiO_2 oxide layer gives way to the formation of Li_2O and Li_4SiO_4 phases at the surface through the reaction with lithium. Then, during cycling the fluorhydric acid (HF), formed by the salt $LiPF_6$ reacting with the traces of water present in the electrolyte, attacks the particles' surface. The disappearance of Li_2O and the fluoration of the surface to give SiO_xF_y (Figure 1.13) are then observed [PHI 13a]. This change in the surface's chemical nature thus eventually disrupts the grafting process of the CMC binder to the surface of the Si particles described previously. In conclusion, one of the main ways of improving performances at present relies on the formulation of electrolytes with, on the one hand, research into additives enabling the SEI to be stabilized and, on the other hand, salts that produce less HF in the electrolyte [PHI 13b].

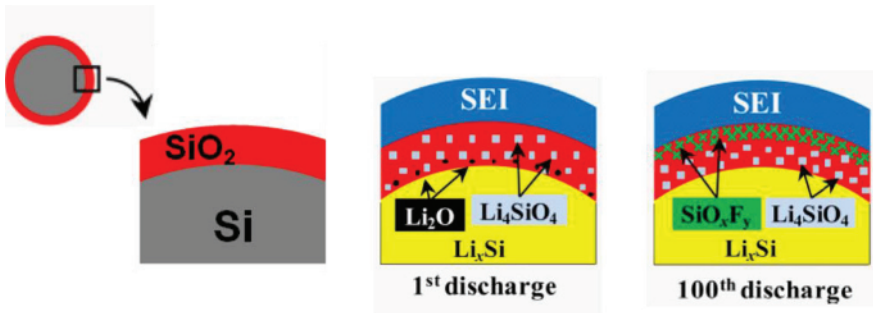

Figure 1.13. *Phase transformations and special reactivity of silicon particles' surface involving the native SiO_2 oxide layer. Formation of Li_2O and Li_4SiO_4 phases at the first lithiation. Fluoration of the surface (SiO_xF_y) and disappearance of Li_2O during cycling following the reaction with HF present in the electrolyte. (Adapted from [IDO 97] with permission. Copyright 2013 American Chemical Society)*

1.3.2. *Other block p elements*

1.3.2.1. *The alloys*

1.3.2.1.1. Tin

In 1997, tin-based amorphous composites were first marketed by Fuji as promising negative electrode materials [IDO 97]. Since that time, numerous studies have focused on the elements from columns 14 to 15 of the periodic table (Ge, Sn, Sb and P) other than Si as possible negative electrode AMs for Li-ion batteries. Just as for silicon, numerous lithiated alloys exist for these elements. For Sn, nine Li_xSn_y alloys can be counted, of which the least lithiated is Li_2Sn_5 and the most lithiated is $Li_{22}Sn_5$.

A lithiation mechanism has been suggested using *in situ* TEM analysis. A sequential phase transformation has been identified involving gradual insertion of Li into the tin grains, which happens reversibly when the Li is deinserted (Figure 1.14). During the first stage, the crystalline tin (beta phase, quadratic space group I41/amd), with a relatively open structure, accommodates the Li ions until the crystallized phase Li_2Sn_5 is formed. In the second stage, Li_xSn_y phases, including the $Li_{22}Sn_5$ phase, form, accompanied by a dramatic volume expansion (~300%).

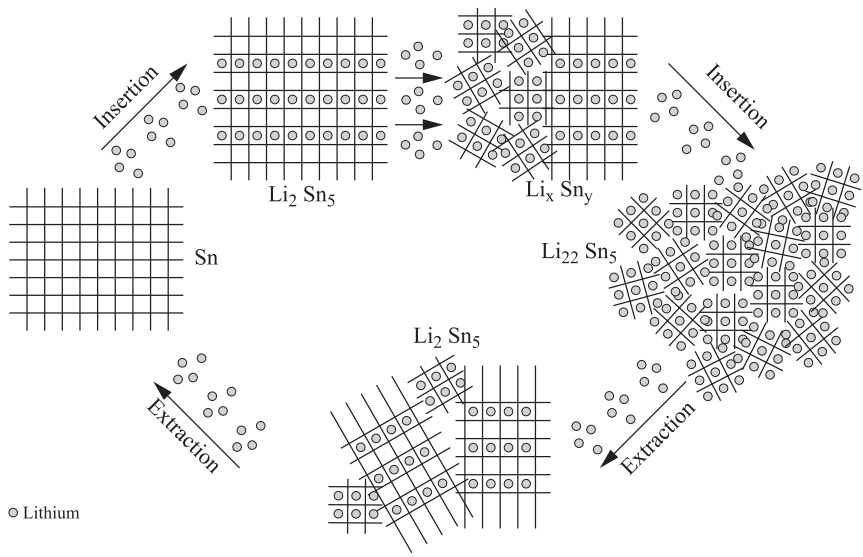

Figure 1.14. *Diagram of electrochemical reactions during Sn lithiation/delithiation. (Reprinted from [LI 14c] with permission. Copyright 2014 American Chemical Society)*

1.3.2.1.2. Antimony and phosphorus

Antimony and phosphorus react very easily with lithium to form Li_2Sb and Li_3Sb (allotropic forms α and γ), and LiP and Li_3P phases, respectively. The theoretical capacities range from 2,596 to 660 mAh/g for P and Sb, respectively, but these high capacities cannot usually be sustained for more than a few cycles. As for silicon, many methods have been developed to address the issue of the loss of contact between the grains of the AM (X = Sn, Sb, P…) in the electrode, which is a consequence of strong volume variations (100–200%). The preparation of X/carbon composites, X'_aX_b (X and X' forming alloys with Li), or M_aX_b compounds (M, transition metal,

not forming any alloy with Li) has meant that significantly improved cycling performances can be achieved. In the case of M_aX_b, the discharge reaction results in a transformation of the initial phase M_aX_b into a composite made up of the lithiated alloy and metallic nanoparticles, M^0:

$$M_aX_b + nb\ Li \rightarrow aM^0 + b\ Li_nX \quad [1.1]$$

Two scenarios can occur during the delithiation upon charge, either (1) the element M remains in the reduced state M^0 and is no longer involved in the charging process, which is referred to as an alloying reaction ($X \leftrightarrow Li_nX$) for the following cycles or (2) the metallic particles, particularly reactive as a result of their nanometric size, are reoxidized in charge to form a $M_{a'}X_{b'}$ phase (eventually, $M_{a'}X_{b'} = M_aX_b$) and this is then referred to as a reversible conversion reaction.

$$aM^0 + b\ Li_nX \rightarrow aM^0 + b\ X + nb\ Li \quad [1.2]$$

$$aM^0 + b\ Li_nX \rightarrow M_{a'}X_{b'} + nb\ Li \quad [1.3]$$

In the first case, the role of M can be beneficial due to (1) the buffering effect of the metallic nanoparticles which enables the volume variations to be absorbed during repeated cycling and (2) the electrode's electronic conductivity to be improved.

1.3.2.2. *The conversion materials*

After being demonstrated for the first time for transition metal oxides [POI 00], the conversion reaction (equation [1.3]) has since been expanded to a number of other elements (X = O, S, P, F, Sb…). This profound transformation of the initial material M_aX_b into a composite electrode made up of metallic nanoparticles and a Li_nX matrix enables high energy densities to be reached. Moreover, it involves redox reactions very different from those of the insertion mechanisms, which only involve the transition metal, whereas here the transition metal and post-transitional element are simultaneously reduced or oxidized. These conversion reactions thus enable more than 1 Li ($1e^-$) to be exchanged per metallic atom, and result in gravimetric and volumetric capacities that can reach 1,000 mAh/g, and 7,000 mAh/cm^3, respectively, which is nearly 10 times that of graphitic carbon (800 mAh/cm^3). Until recently, these materials were only a laboratory curiosity since the conversion reaction, although reversible, did

not result in useful cyclabilities. This drawback has nevertheless been partially lifted due to (1) a good understanding of the limiting mechanisms at the electrode/electrolyte interfaces and (2) a better formulation of the electrode enabling on the one hand, the volume variations in the electrode to be absorbed and on the other hand, the electrode's electronic percolation to be improved. This conversion mechanism can sometimes be preceded by an insertion stage forming an intermediate phase. This has been shown to be the case for CuO. The intermediate phase Cu_2O is observed before the conversion into Cu and Li_2O nanoparticles [DÉB 01, XIA 09]. In the case of the sulfide FeS_2, an intermediate phase $Li_{2+x}Fe_{1-x}S_2$ is formed before the conversion into Li_2S and Fe nanoparticles [GOL 99, STR 03]. Note that polysulfide intermediate phases, partially soluble in the electrolyte and resulting in a decrease in the electronic conductivity, represent a serious limitation for this system [AUR 09, YAM 83].

This intermediate phase may only appear after an initial discharge, this is the case for FeP for which a direct conversion reaction occurs (equation [1.4]) during the initial discharge, while a double insertion/conversion process comes into play during the subsequent discharges and charges according to equations [1.5] and [1.6].

First discharge: $FeP + 3\,Li \rightarrow Li_3P + Fe$ [1.4]

During cycling: $Li_3P + Fe \leftrightarrow LiFeP + 2Li$ [1.5]

$LiFeP \leftrightarrow FeP + Li$ [1.6]

1.3.2.3. *Limitations: volume changes and instability of the SEI*

As with silicon, the volume changes that occur during the electrochemical process and result in a rapid drop in the battery's reversible capacity represent the main problem with those systems based on post-transitional elements. Tin can be used as an example to illustrate the phenomenon of volume expansion. During the second stage of lithiation for Sn, the phases Li_xSn_y including the phase $Li_{22}Sn_5$ nucleate, accompanied by dramatic volume expansion (shown in Figure 1.15). Pulverization occurs during delithiation by an agglomeration of vacuums, demonstrating a different mechanism to that governed by fractures for silicon [LI 14c].

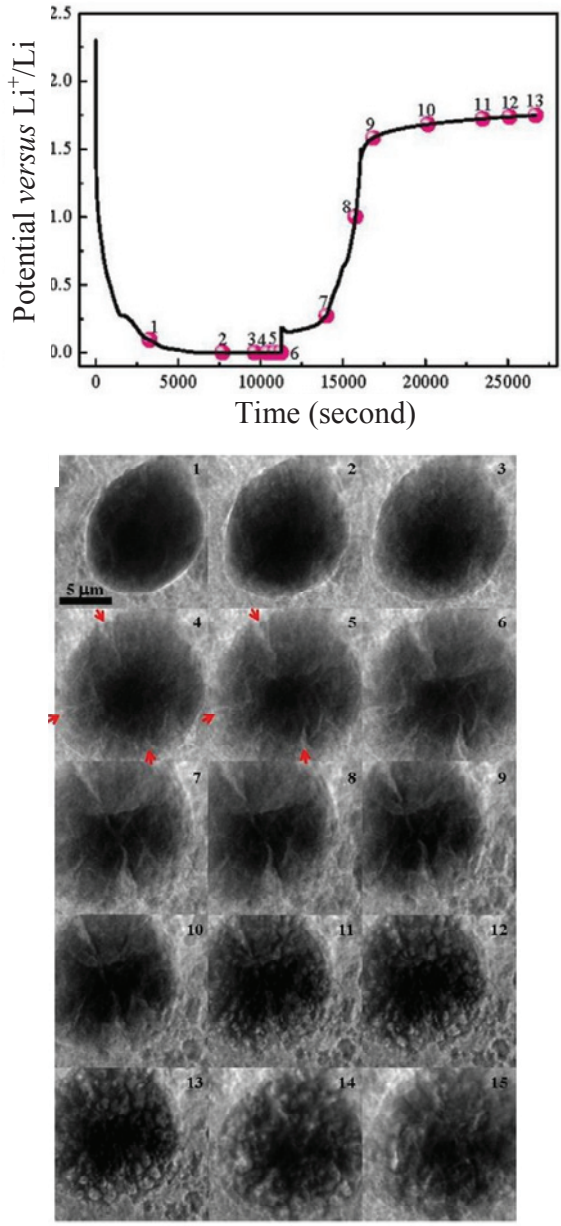

Figure 1.15. *Illustration of fissures formed in tin grains during the first cycle: a) potential curve as a function of time with points where b) the in situ X-ray transmission microscopy images were recorded. (Adapted from [CHA 10] with permission. Copyright 2010 Elsevier). For a color version of the figure, see www.iste.co.uk/dedryvere/electrodes.zip*

Figure 1.15 illustrates the dynamic for the expansion of Sn particles during lithiation (points 1–6), during which a clear lithiated zone can be seen along the particles' contour, separated from the darker core of the Sn particle by a more diffuse (non-lithiated) area. The clear zone becomes thicker and thicker during lithiation, the dark core diminishes and the size of the particle increases. The existence of this core-shell mechanism suggests that the alloy process is not limited kinetically by the diffusion of Li ions but by the biphasic reaction (Sn/Li_xSn) at the interface. The arrows on the microscopy slides (Figure 1.15) indicate the numerous fissures that appear, demonstrating the fragile nature of the Li_xSn phases in contrast to Sn's initial ductility. A total volume expansion of 380% has been recorded, which is very close to the theoretical expansion calculated from Sn and $Li_{22}Sn_5$ lattice cells (359%). During charge, a clearer image (points 6–13) can be observed, indicating that the porous particles are being reconstructed (the Sn is being aggregated) which is combined with a volume decrease, limited to 10%.

As for silicon, these repeated volume changes give rise to great instability in the SEI, which has to form continually on a surface that is perpetually being reconstructed, given that at low potential each portion of the surface newly exposed to the electrolyte must be passivated. A continuous consumption of lithium, which is synonymous with a loss of reversible capacity, follows along with an increase in the battery's impedance, resulting from the pores being blocked by products formed by the degradation of the electrolyte. Therefore, the same kinds of strategies to improve performances in cycling are used as when working with silicon.

1.3.2.4. *Nanostructuration*

Even though it is difficult to envisage for industrial production, the nanostructuration of phases based on post-transition elements (MA=Sn, Sb, P…) enables performances during cycling to be improved. As for Si, this improvement is due to the shortening of diffusion pathways for Li (which enables the capacity and cycling kinetics to be improved), to the larger contact surface between the AM and the current collector (an improvement in the electronic conductivity) and to the larger exchange surface between the AM and the electrolyte, which increases ionic conductivity. The reduction in the size of the particles also facilitates the phase transitions which accompany the conversion or formation of alloys, which can reduce the fractures within the electrode [BRU 08]. There are many examples demonstrating the interest of growing AMs on nanometric metallic

substrates, such as Fe_3O_4 or Ni_3Sn_4 on Ni nanorods, [TAB 06, HAS 07] or Cu_3P on Cu nanorods, foils or foams [GIL 05, BOY 08]. Such approaches enable power and cyclability to be increased considerably and also make the addition of conducting carbon additives unnecessary.

In the same approach to improving electrochemical properties versus lithium, the material's initial porosity can be an interesting property to use. The porous structure of Fe_2O_3 has thus been advantageously used recently to accommodate this phase's volume changes during reactions with lithium, and so to maintain its integrity and performance during cycling [XU 14b]. Similar benefits can be obtained similarly with macroporous architectures, for example, for NiO [WEN 13]. The use of a porous carbon matrix can also enable the volume changes in the AM to be absorbed (AM is confined in the porous carbon), as well as activating the material's reactivity toward lithium. Red phosphorus, for example, displays an extremely high theoretical capacity of 2,596 mAh/g, but because of its weak electronic conductivity it makes only a poor electrode material. Using a simple vaporization-condensation process of phosphorus in the porosity of a mesoporous carbon, it is possible to activate P's electrochemical properties versus lithium. Under these conditions, a capacity of 2,000 mAh/g can be maintained over hundreds of cycles [MAR 11, WAN 12]. Combining intermetallic phases with graphene sheets can also be very effective [LU 12].

Despite the obvious cost limitation of these different syntheses, and the weak energy density due to the small quantity of AM in this type of composite, the improvements in performance are promising, especially in terms of cyclability and kinetics.

1.3.2.5. *Electrode formulation*

As for Si, cyclability remains limited by (1) the precipitation of degradation products from the electrolyte and (2) the variation in the electrode's texture resulting from the volume expansion of particles which results in the AM grains becoming electrically disconnected from each other and from the conductive additive (carbon). The electrodes must be very porous to allow the AM particles to "breathe" during cycling. The results obtained, for example, with the conversion material TiSnSb with an electrode with 45% porosity (brought by the electrode formulation), are unanimous as shown in Figure 1.16 with a gravimetric capacity of 700 mAh/g and a volumetric capacity of 850 mAh/cm^3 (greater than that of

Cgr 550 mAh/cm^3 for an electrode displaying a porosity of 30%) being maintained after hundreds of cycles, whereas without formulation the capacity is totally lost after 50 cycles.

Formulating electrodes based on CMC also enables a very good distribution of grains of active matter on different scales by forming a network in which carbon and the AM (Sn, Sb, P, etc.) are organized. The carbon fibers sometimes used (VGCF) to ensure adherence on the current collector and therefore, the cycling capacity can be better maintained [SIV 11].

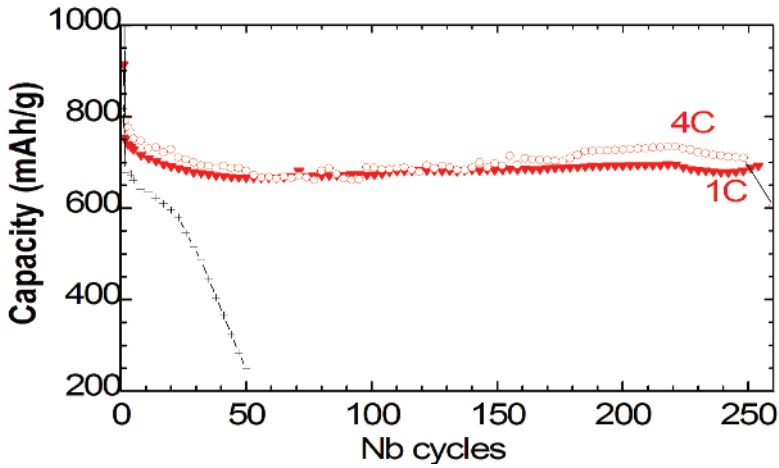

Figure 1.16. *Performances of the TiSnSb composite electrode (CMC/C_B+VGCF) at different cycling rates (4C and C) compared to an electrode prepared without CMC binder*

Finally, due to an optimized electrode formulation, high surface capacities (e.g. 3.0 mAh/cm² for TiSnSb, equivalent to 500 mAh/g) can be reached at a slow rate with thick electrodes (e.g. 6 mg of TiSnSb by square centimeter of electrode), demonstrating that intermetallic phases can rival the practical volumetric capacities of silicon. Indeed, although silicon shows a much greater theoretical capacity (3,578 mAh/g) than intermetallic phases based on Sn and Sb, in practice these electrodes only function correctly with a low loading in Si (rarely more than 1–2 mg/cm²).

1.3.2.6. *Electrolyte formulation: the effect of additives*

It is also possible to improve performances by the use of additives in the electrolyte [WIL 12]. In some cases, adding FEC to the electrolyte permits a distinct increase in the cyclability of an electrode based on intermetallics. Impedance spectroscopy has shown that the addition of FEC to the electrolyte decreases the SEI's resistance during cycling (the SEI is not so thick here), as well as the charge transfer resistance between the SEI and the AM. The improvement brought about by adding FEC is not limited to sustaining capacity over cycles, adding FEC also seems to minimize the degradation of the electrolyte and its consequences [JAN 13].

Although the use of additives in the electrolyte is a simple way of improving performances, research into new solvents and salts should not be neglected, as recently demonstrated in copper sulfate-based electrodes for which the use of an ether-based electrolyte (e.g. 1 M lithium bis(trifluoromethanesulfonyl)imide (LiTFSI) in dioxolane/dimethoxyethane (DOL/DME)) has brought about a distinct improvement in sustaining capacity and coulombic efficiency [JAC 14].

1.4. Summary on negative electrodes

This chapter has indicated the main lines of research favored for increasing the performances of negative electrodes for Li-ion batteries. The requirements (see Table I.1) for negative electrodes are many and depending on the priority given to them, the negative electrode materials discussed meet them only partly. Each material, depending on its properties, may be suitable for a very specific niche application. Thus, titanium oxides, which show moderate capacities but a good charge/discharge kinetics, cost relatively little and are not toxic, could meet industrial needs for batteries for portable electronics, whereas materials based on post-transitional elements, demonstrating high gravimetric and volumetric capacities but limited kinetics, would be better suited to large-scale stationary storage. Note that many of these post-transitional elements (Sn and Sb) are becoming scarcer, which limits their future use in batteries.

Moreover, performances are greatly improved by an electrode formulation adapted to each material which, by improving electronic percolation and ionic conductivity, enables the redox system provided by the

AM to work, even if this does not inherently possess the required properties (electronic conductivity and Li diffusion).

Research always focuses on increasing energy densities and therefore, specific capacities, nevertheless these depend on the cathode used, which is the limiting electrode in terms of capacity in Li-ion batteries. Chapter 2 seeks to describe the main positive electrode materials.